Dynamics of ring current ions as obtained from IMAGE HENA and MENA ENA images

J. D. Perez and X.-X. Zhang[1]
Physics Department, Auburn University, Auburn, Alabama, USA

P. C:son Brandt and D. G. Mitchell
Applied Physics Laboratory, John Hopkins University, Laurel, Maryland, USA

J.-M. Jahn and C. J. Pollock
Southwest Research Institute, San Antonio, Texas, USA

Received 25 July 2003; revised 2 February 2004; accepted 20 February 2004; published 11 May 2004.

[1] Ion distributions from three storms in the year 2000 have been obtained from HENA and MENA ENA images at 27–39 keV and 5–12 keV, respectively. The observed motion of the ring current is compared with calculations of expected radial and angular drift speeds made using a combination of the Tsyganenko 89 magnetic field model and the Weimer 2001 electric field model. In one case between 1000 and 1100 UT on 10 June 2000 that had already been reported, the westward drift of the 33 keV ions is as expected. Comparisons with speeds inferred from the motion of peaks in the ion distributions, however, often did not agree with the model predictions. Examination of the predicted paths showed that the ions are expected to experience significant energy changes as they drift so that they quickly move out of the observed energy channel. Thus we are able to conclude that the observed motion is consistent with equatorial electric fields in the inner magnetosphere of a few tenths of a mV/m on 10 June 2000, several mV/m on 12 August 2000, and $\leq$1 mV/m on 4 October 2000 as predicted. Other interesting observations include (1) the suggestion of a two step injection process during the main phase of the 4 October 2000 storm, (2) the unexplained disappearance of the 33 keV protons when their drift motion brings them to noon in the recovery phase of the 10 June 2000 storm, (3) the apparent subtle changes in the electric potential pattern in the equator early in the 4 October 2000 storm, and (4) the energy dependence of the spatial source of the injected particles in the plasma sheet during the strong storm on 12 August 2000. *INDEX TERMS:* 2730 Magnetospheric Physics: Magnetosphere—inner; 2778 Magnetospheric Physics: Ring current; 2794 Magnetospheric Physics: Instruments and techniques; 2712 Magnetospheric Physics: Electric fields (2411); *KEYWORDS:* ENA imaging, ring current, storm

Citation: Perez, J. D., X.-X. Zhang, P. C:son Brandt, D. G. Mitchell, J.-M. Jahn, and C. J. Pollock (2004), Dynamics of ring current ions as obtained from IMAGE HENA and MENA ENA images, *J. Geophys. Res.*, *109*, A05208, doi:10.1029/2003JA010164.

1. Introduction

[2] Large spatial scale electric fields are responsible for the acceleration of ions that are injected from the plasma sheet into the Earth's ring current and their subsequent convection in the inner magnetosphere. Values of these fields have been inferred from measurements made in the ionosphere using radar and along the paths of low-altitude satellites in polar orbit by mapping along magnetic field lines and have been measured directly by satellites whose orbits traverse the inner magnetosphere. *Wygant et al.* [1998] summarized past work and presented extensive data from the CRRES satellite that showed the penetration of large fields with magnitudes greater than 1 mV/m during the main phase of geomagnetic storms and subsequent shielding of the fields by ring current ions that kept the fields from reaching earthward of L = 4 R_E. *Whipple et al.* [1998, 1999] applied a technique based on (U, B, K) coordinates to correlate particles observed by multiple satellites and to identify particles that were observed by a single satellite at different points along its path through the inner magnetosphere. From the observed motion they were able to infer electric fields that were in agreement with values obtained from the combination of the Tsyganenko 1996 magnetic field model [*Tsyganenko*, 1995] and the Weimer 96 electric potential model [*Weimer*, 1996]. *Korth et al.* [1999] displayed data from the magnetospheric plasma analyzer (MPA) instrument on Los Alamos geosynchronous satellites as a function of local time and *Kp* to show distinct

[1]Currently at Alabama A & M University, Normal, Alabama, USA.

0148-0227/04/2003JA010164

boundaries in the fluxes that are consistent with particle drift processes that are due to the corotational and a screened dawn-to-dusk electric field. *Korth et al.* [2000] used CRRES data to report electric fields as a function of magnetic local time during the main phases of storms with approximately 5 hour time resolution, but *Korth and Thomsen* [2001] found that geosynchronous orbit data cannot distinguish between a screened dawn-dusk convection electric field and more sophisticated models.

[3] Energetic neutral atom (ENA) imaging can provide a comprehensive view of the motion of trapped ions in the inner magnetosphere [*Williams et al.*, 1992; *Gruntman*, 1997]. The first results using this technique [*Roelof*, 1987] showed a strong midnight/noon intensity asymmetry during a geomagnetic storm. *Henderson et al.* [1997] saw a ring of enhanced ENA emission encircling the Earth during a storm on 29 August 1996 and ENAs associated with a substorm on 31 July 1996. *Jorgensen et al.* [1997] integrated over ENA images to show that the ENA intensity is related to *Dst*. *Henderson et al.* [1999] saw both a noon-midnight and dawn-dusk asymmetry of the ring current in ENA images. *C:son Brandt et al.* [1999] used ENA images taken from low altitude to observe precipitating ions from $L \geq 6\ R_E$ and show that their intensity is related to *Kp* and *Dst*. *C:son Brandt et al.* [2002e] found from Astrid-1 ENA images that plasma may be convected from the plasma sheet in narrow channels.

[4] The Imager for Magnetopause-to-Aurora Global Exploration (IMAGE) satellite [*Burch*, 2000] provides ENA images from high altitude with enhanced spatial resolution and greater energy coverage. Much has been learned from the ENA images themselves. In High Energy Neutral Atom (HENA) [*Mitchell et al.*, 2000] images, *Mitchell et al.* [2001] found injections that reached $L \sim 3\ R_E$ in a strong storm on 15–16 July 2000 but only $L \sim 7\ R_E$ in a minor storm on 10 June 2000. In Medium Energy Neutral Atom (MENA) [*Pollock et al.*, 2000] images during a strong storm on 12 August 2000, *Pollock et al.* [2001] showed the evolution of the ring current from a noon/midnight asymmetry during the main phase to a higher degree of symmetry during the recovery phase. *Burch et al.* [2001b] compared the HENA ENA images of the ring current with EUV plasmasphere images to show that the peak of the ring current was nearly centered on the plasmapause during geomagnetic storms on 24 May 2000 and 29 July 2000. *C:son Brandt et al.* [2002b] observed two events in HENA images from 16 to 50 keV during the storm on 23–26 May 2000. One is a sharp decrease in the dayside ring current attributed to a southward turning of the IMF and subsequent increase in the polar cap potential that changes the ion drift paths. A second is an observation of a spatial correlation between the ring current and the plasma pause on the dayside during the recovery phase of the 24 May 2000 storm. It is the same event analyzed by *Burch et al.* [2001b]. The lack of ENA emissions on the duskside was attributed to pitch angle distributions peaked around 90° as result of wave-particle interaction with ion cyclotron waves.

[5] Inverting the ENA images to obtain equatorial ion distributions yields even more information about the Earth's inner magnetosphere. *Perez et al.* [2001] using ENA images from HENA during a weak storm on 10 June 2000 and from MENA during a strong storm on 12 August 2000 demonstrated the ability to extract ion distributions from ENA images but did not include the contributions from charge exchange with neutral oxygen at low altitudes. *Burch et al.* [2001a] showed energy dependent drift from 1100 to 1200 UT on 4 June 2000 from MENA and HENA images. *C:son Brandt et al.* [2002a] inverted HENA images integrated over energy from 10–60 keV to demonstrate that plasma sheet emissions beyond 8 R_E diminish and that the ions are pushed into $L = 4\ R_E$ during substorm dipolarizations. During a number of storms, *C:son Brandt et al.* [2002c] determined the location of the maximum ion flux from HENA ENA images. Most of the time the location of the peak was in the postmidnight sector for the 27–60 keV ions, which implied motion of the ions due to twisted electric equipotentials as modeled by *Fok et al.* [2001]. *C:son Brandt et al.* [2002d] inverted HENA 27–60 keV ENA image from 0800 to 0900 UT on 4 October 2000 to conclude that the observed proton drop out was due to a substorm dipolarization. Earlier, 0640 and 0830 UT, and later, 1721 and 1930 UT, during the same storm, *C:son Brandt et al.* [2004b] found that the inverted ion distributions show that substorms do not necessarily increase the energy content of the ring current in the energy range below 80 keV. MENA images showed a similar morphology. In the most ambitious use of inversions of ENA images to date, *C:son Brandt et al.* [2004a] use inversions of ENA images to infer pressure gradients and currents from the ring current to the ionosphere.

[6] In this paper, we will examine and/or reexamine in greater detail the ion drifts as obtained from MENA and HENA ENA images during (1) the recovery phase of the weak storm on 10 June 2000, (2) the period just after the beginning of the recovery phase of the strong storm on 12 August 2000, and (3) early in the main phase of the storm on 4 October 2000. As mentioned above in this section, these storm times have been examined previously. Here we will show new inversions of the ENA images and examine the motion of representative ion guiding centers at the peaks of the distributions. The observations will be compared to electric fields predicted by a combination of the Tsyganenko 89 [*Tsyganenko*, 1989] magnetic field model and the Weimer 2001 [*Weimer*, 2001] electric field model.

[7] In section 2 we will briefly review the methodology used to invert the ENA images. In section 3 we will present the observations from the three storms, and in section 4 we will discuss the implications of the observations. Section 5 contains a brief summary along with the conclusions.

2. Inversion of ENA Images

[8] The ENA images obtained by HENA and MENA can be represented by the number of neutral atoms (H for the ones presented in this paper.) in pixel α, i.e., C_α, which can be expressed in terms of the following integral:

$$C_\alpha = \int d^3\ x\ dE\ \ d\Omega\ dt\ f(\vec{x},\vec{v})\sigma_{ex}(E)\rho_n(\vec{x})R_\alpha,$$

where d^3x is the volume element of the line-of-site of each pixel, dE is the energy interval over which the pixel responds, $d\Omega$ is the solid angle of velocities accepted by the pixel, dt is the time for collecting neutrals, $f(\vec{x}, \vec{v})$ is the ion

flux, $\sigma_{ex}(E)$ is the appropriate charge exchange cross section, $\rho_n(\vec{x})$ is the density of the appropriate neutral species, and R_α is the response function of the pixel. The problem of extracting the unknown ion flux f from the neutral counts is a standard mathematical inversion problem for which there are different approaches to finding a solution [*Perez et al.*, 2000; *Roelof and Skinner*, 2000; *C:son Brandt et al.*, 2004b].

[9] The ion fluxes presented in this paper are extracted from the ENA images by assuming that the ions are on closed field lines on which energy and magnetic moment are conserved so that the three spatial dimensions and the three velocity dimensions can be reduced to an equatorial pitch angle distribution, i.e., two spatial dimensions, r and φ_{MLT}, and velocity pitch angle ψ. Then the unknown is expanded in terms of cubic B-splines [*deBoor*, 1978], i.e.,

$$f_{eq}(r, \varphi_{MLT}, \cos\psi) = \sum_{i,j,k} a_{i,j,k} S_i(r) S_j(\varphi_{MLT}) S_k(\cos\psi).$$

The expansion coefficients $a_{i,j,k}$ are determined from the linear minimization condition,

$$\delta(\chi^2 + \lambda P) = 0.$$

The χ^2 is defined as

$$\chi^2 \equiv \frac{1}{N} \sum_{\alpha=1}^{N} \left(\frac{C_\alpha - c_\alpha}{\sigma_\alpha} \right)^2,$$

with c_α as the counts in pixel α calculated with the expansion coefficients $a_{i,j,k}$, and σ_α as the uncertainty in pixel α. The χ^2 measures the degree to which the ion distribution fits the data. The P, called the penalty function, measures the smoothness of the solution. The long, complicated expression for P is given by *Perez et al.* [2001]. It is based upon Bayesian statistics and was derived by *Wahba* [1990]. It involves combinations of the derivatives up to second order with respect to the variables, r, φ_{MLT}, and cosψ. The parameter λ balances the need to fit the data and to make the distribution function smooth. It is chosen so that χ^2 is one, i.e., we make f as smooth as possible while still fitting the data.

[10] The following should be noted in interpreting the results of this inversion process:

[11] 1. Contributions from neutrals created by charge exchange with ions on open field lines are not included in the analysis. The number of such neutrals in the observed images is expected to be small.

[12] 2. Contributions are included for charge exchange with neutral hydrogen in the geocorona at altitudes above 1000 km. The charge exchange cross section for H^+ on H is taken from *Barnett et al.* [1990]. The geocoronal density is the spherically symmetric *Chamberlain* [1963] model below 3.5 R_E and the asymmetric *Ostgaard et al.* [2003] model above 3.5 R_E. The latter is taken from FUV images on IMAGE and provides an increased neutral hydrogen density in the tail. We find just as did *C:son Brandt et al.* [2002a] that the asymmetry improves the inversion results.

[13] 3. Contributions are included for charge exchange with neutral hydrogen and oxygen between 100 and 1000 km altitude. The charge exchange cross section for H^+ on O is taken from *Stancil et al.* [1999]. The densities of neutral hydrogen and oxygen, which are taken from the MSISE90 model [*Hedin*, 1991], vary in three dimensions and depend on the F10.7 radiation from the sun index and the Ap geomagnetic activity index. Since the emission of the ENA after charge exchange is no longer "optically thin" at these altitudes, an approximate "opacity" factor is included. Changes of the lower altitude from 100 to 500 km have been found to have no significant effect on the results. Owing to the addition of the effects of charge exchange with neutral O, the results presented in this paper differ somewhat from those in the work of *Burch et al.* [2001a] and *Perez et al.* [2001]. While these low altitude emissions do contribute to the ENA images treated in this paper, they are usually not the dominant emissions.

[14] 4. The uncertainties in the data, σ_α, have been estimated as the square root of the counts. This is most certainly not completely correct, but it seems to give a good estimate of the relative uncertainties in the HENA data. For the MENA data, we found that it was necessary to establish a minimum uncertainty of approximately 5 counts.

[15] 5. The number of expansion functions is usually 10 radial cubic splines forced to be zero at the minimum and maximum radius, 8 periodic cubic splines, and 4 cosine of the pitch angle cubic splines for a total of 320. These are not all independent parameters due to the regularization condition imposed by the penalty function [*Press et al.*, 1992]. They do, however, provide an extremely general description of the spatial dependence of the ion distribution and a pitch angle distribution that can vary from point to point. The minimum radius is chosen to be 2 R_E and the maximum radius is either 8 or 10 R_E.

[16] 6. Since the ions are trapped on closed field lines, we take both the forward and backward loss cone in the pitch angle distribution to be empty. Prior to including the contributions from charge exchange with low altitude oxygen, there were indications that the data required filling the loss cone [*Perez et al.*, 2001], but the angular resolution of the images is not really adequate to resolve such details of the pitch angle distribution.

[17] 7. The equations that result from the minimization condition above are linear and therefore easy to solve, but they allow the resulting ion distribution to be negative. Enforcing a positivity constraint would yield nonlinear equations to determine the expansion coefficients. Clearly, the physical ion distributions are positive definite, so when there is enough information in the data, the resulting distributions are positive. It has been found that from certain viewing positions, the ENA images do not yield acceptable ion distributions because only a small portion of the pitch angle distribution at some locations on the equator is effectively constrained by the data. This restricts the time periods during which valid ion distributions can be obtained from the ENA images. In the results that follow, there will be occasional white areas in the plotted ion distribution functions where it has swung negative. In all cases shown, the smallest negative value is much less than the highest positive value.

[18] Figure 1 shows an example of an inversion for a HENA ENA image from 27 to 39 keV on 4 October 2000 at 0745 UT. Figure 1a shows the ENA image projected

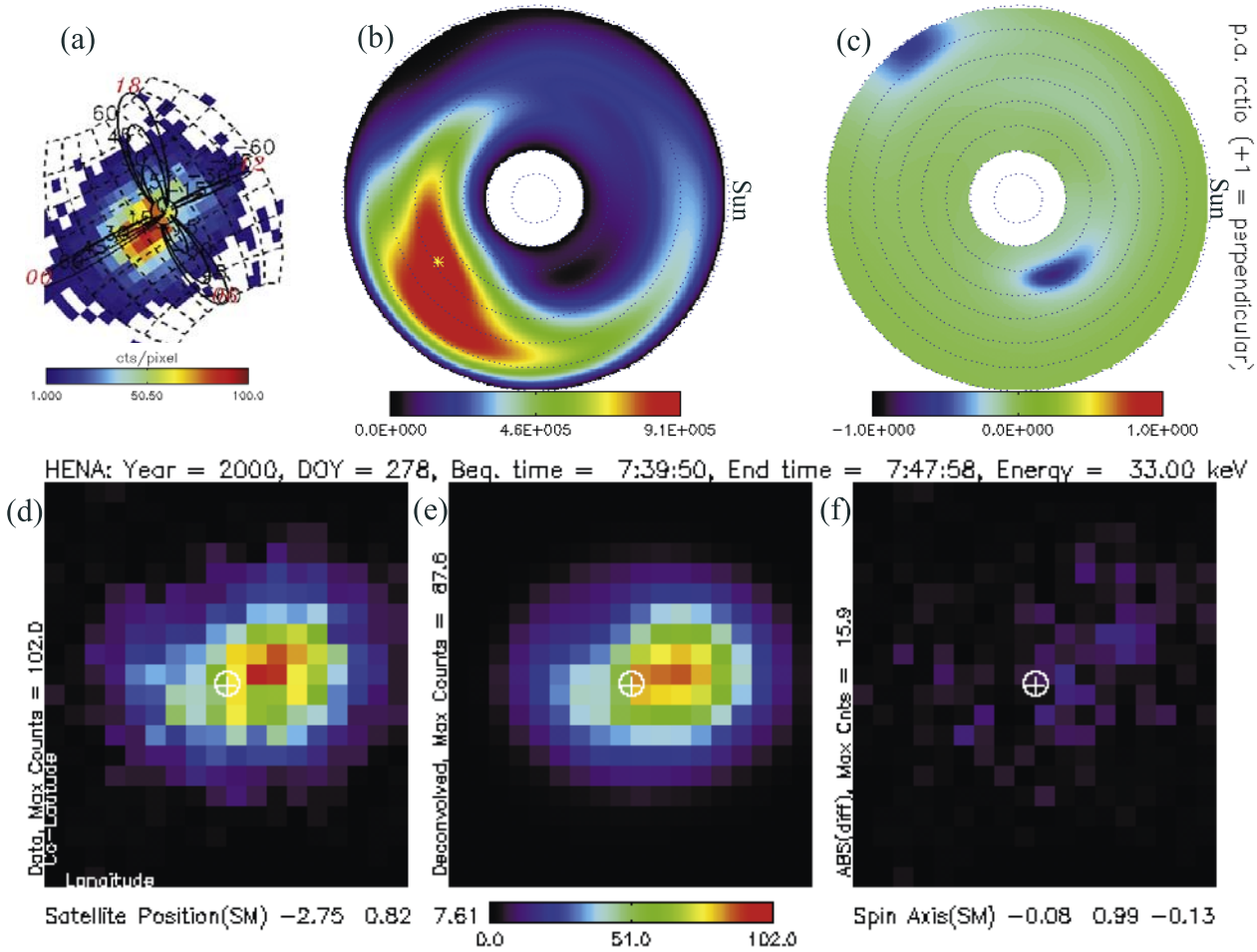

Figure 1. Example of the results of an inversion of a HENA image at 0745 UT on 4 October 2000. Plot of HENA data in Figure 1a is from the HENA web site http://sd-www.jhuapl.edu/IMAGE/.

onto a grid in instrument coordinates with dipole field lines at 3, 6, and 9 R_E at midnight, dawn, noon, and dusk to guide the eye. The Sun is toward the upper right. The ENA emissions peak between midnight and dawn in pixels that are within 3 R_E of the Earth in this projected view. The inverted equatorial ion flux in ions/(keV s cm^2) integrated over all pitch angles is shown in Figure 1b. The peak in the flux is marked by a yellow star and occurs at 5 R_E. (Dotted circles are at 1 R_E intervals.) This is farther from the Earth than the peak in the ENA flux because of the motion along field lines of the ions and the convolution with the geocoronal hydrogen density in the ENA flux. Figure 1c shows the pitch angle anisotropy defined as

$$A \equiv \frac{J_\perp - J_\parallel}{J_\perp + J_\parallel}, \quad J_\perp \equiv \int_0^{1/2} f_{eq} d(\cos\psi), \quad J_\parallel \equiv \int_{1/2}^{1} f_{eq} d(\cos\psi).$$

Except in regions of very low flux, the pitch angle distributions as they do here almost always appear nearly isotropic. This is more a reflection of the fact that the angular resolution of the ENA images does not provide enough information to extract details of the pitch angle distribution rather than the fact the pitch angle distributions are always isotropic in the ring current. The data in Figure 1a, i.e., the C_αs in the equations above, are replotted in Figure 1d as a rectangular array of pixels. In Figure 1e the counts per pixel calculated using the equatorial ion distribution in Figures 1b and 1c, i.e., the c_αs in the equations above or the simulated ENA image using the retrieved ion distribution, are plotted. We see that the main features of the data are reproduced, and the fit is not perfect as is to be expected from a $\chi^2 = 1$. The absolute value of the difference between the data and the calculated values, i.e., $|C_\alpha - c_\alpha|$ is plotted in Figure 1f. The maximum number of counts in any pixel in Figure 1f is 15.9, and we see that the "errors" do not clump in any particular region.

3. Data From Three Storms

[19] We present ion distributions from three storms in the year 2000. The SYMH and ASYMH indices for each are presented in Figure 2. The SYMH is similar to the *Dst* index so that it describes the strength and time evolution of a geomagnetic storm. *Jorgensen et al.* [1997] showed an

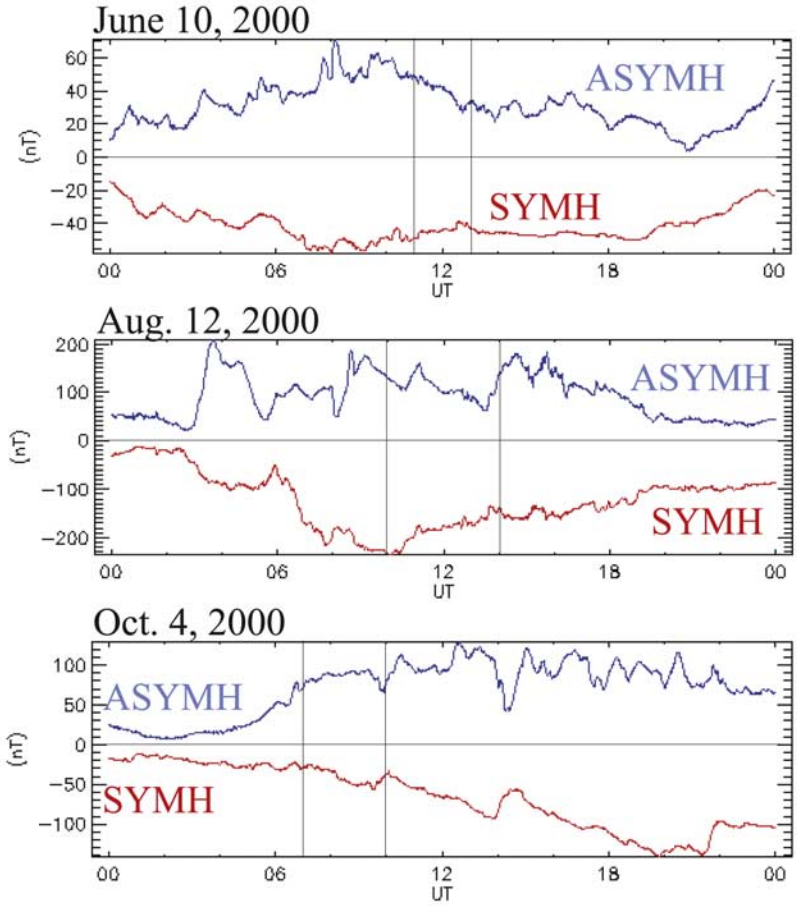

Figure 2. Plot of the geomagnetic indices SYM-H and ASY-H for three storms. The data is from the web site http://swdcdb.kugi.kyoto-u.ac.jp/.

association of *Dst* and global energetic neutral atom measurements. The ASYMH is presented because it correlates well with the *AE* indices as an indicator of substorm activity [*Iyemori*, 1990]. *Jorgensen et al.* [2000] showed that short-lived bursts of ENAs are signatures of substorms. The vertical black lines mark the time periods in which the IMAGE satellite was high above the Northern Hemisphere and for which we were able to perform valid inversions of the ENA images.

3.1. Weak Storm on 10 June 2000

[20] The storm on 10 June 2000 is a relatively weak storm with a minimum SYMH greater than −60 nT. We obtained ion distributions between 1100 UT and 1300 UT in 15 min intervals for 27–39 keV HENA images and 5–12 keV MENA images. By this time, the storm is well into the recovery phase as both SYMH is increasing and ASYMH is decreasing. Plots for 1100, 1200, and 1300 UT are shown in Figure 3. Figures 3a–3c are the ion equatorial fluxes integrated over pitch angle from HENA, and Figures 3g–3i are the ion fluxes from MENA. Figures 3d–3f will be discussed in the next section. We note that in some regions the inverted fluxes from HENA dip slightly negative. The 27–39 keV ions have already drifted to dusk and between 1100 and 1200 UT continue to drift westward and then stop. The ion flux diminishes over the 2 hour period. The 5–12 keV ions have remained near midnight and now drift eastward. There is a rebrightening at 1300 UT.

3.2. Strong Storm on 12 August 2000

[21] The storm on 12 August 2000 is a strong storm with a minimum SYMH below −200 nT. We obtained ion distributions between 1000 UT and 1400 UT in 15 min intervals for the same energy bands. This is the period of time just after the minimum in SYMH at 1000 UT that includes a rise in ASYMH to a local maximum at 1100 UT. Plots for 1000, 1100, 1200, and 1300 UT are shown in Figure 4. Figures 4a–4d are the inverted HENA images and Figures 4i–4k are the inverted MENA images. We were not able to obtain a good inversion of MENA images after 1200 UT. Figures 4e–4h will be discussed in the next section. The 27–39 keV ions peak in the postmidnight/predawn sector. There is no apparent drift. The peak flux coincides with a peak in ASYMH at 1100 UT. The rebrightening at 1300 UT coincides with a small rise in ASYMH. The 5–12 keV ions peak in the postdusk/premidnight sector. Drift of the flux peaks, if there is any, is hard to discern. The flux increases between 1000 and 1200 UT.

3.3. Medium Strength Storm on 4 October 2000

[22] The storm on 4 October 2000 has a long main phase in which SYMH reaches approximately −150 nT. We obtained ion distributions between 0700 and 1000 UT in

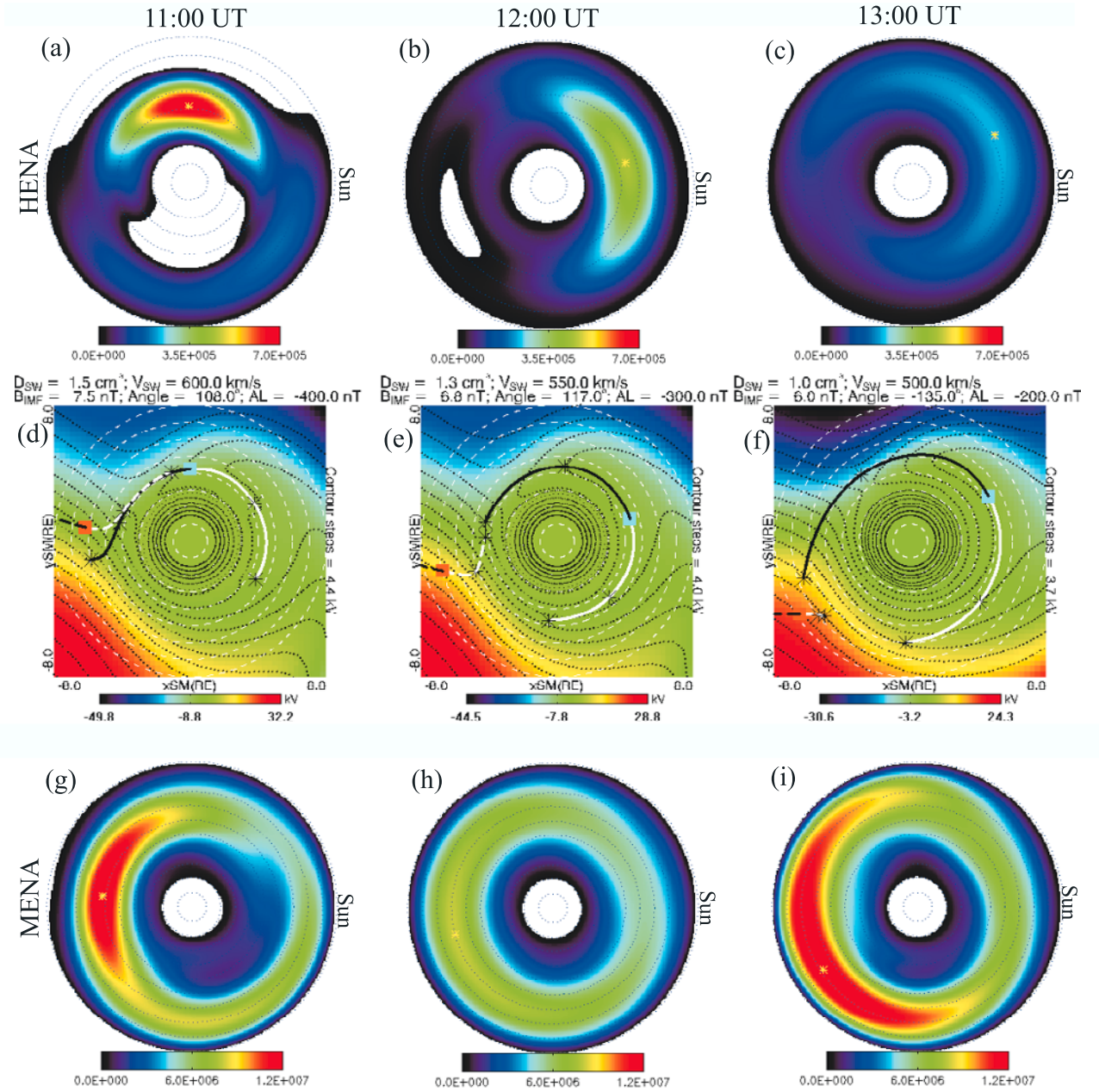

Figure 3. Equatorial ion fluxes integrated over pitch angles (ions/(keV s cm2) for (a)–(c) 33 keV ions and (g)–(i) 5–12 keV ions in 1 hour intervals on 10 June 2000. Figures 3d–3f are model calculations that are explained in the text.

15 min intervals from the 27–39 keV HENA ENA images. The dayside of the MENA images was screened by sunlight so inversions were not performed. Plots for 0700, 0800, and 0900 UT are shown in Figure 5. Figures 5a–5c are the equatorial fluxes integrated over pitch angles. Figures 5d–5f will be discussed in the next section. The 27–39 keV ions peak in the postmidnight/predawn sector. In the ion flux at 0800 UT, there are two peaks in the distribution, one between 4 and 5 R_E and another between 6 and 7 R_E. This is suggestive of a two step injection process in which particles that were injected by a preceding increase in the electric field and are further accelerated and pushed to low L values as a result of a second increase in the electric field as inferred by *Wygant et al.* [1998]. The ASYMH stays fairly constant during this period while the ion flux is decreasing. The peak in the ion flux at 0900 UT appears to move eastward to 0600 MLT, but it is to be noted that the flux is low and the peak is a very weak one.

4. Discussion

[23] If we plot the location of the peak of the ion flux as a function of time, a radial and angular speed can be calculated. The left hand column of Figure 6 shows the radius (blue) and MLT (red) of the peaks in the ion distributions for the three storm periods of time for which we were able to obtain valid inversions of the HENA and MENA ENA images. The right hand column of Figure 6 shows the

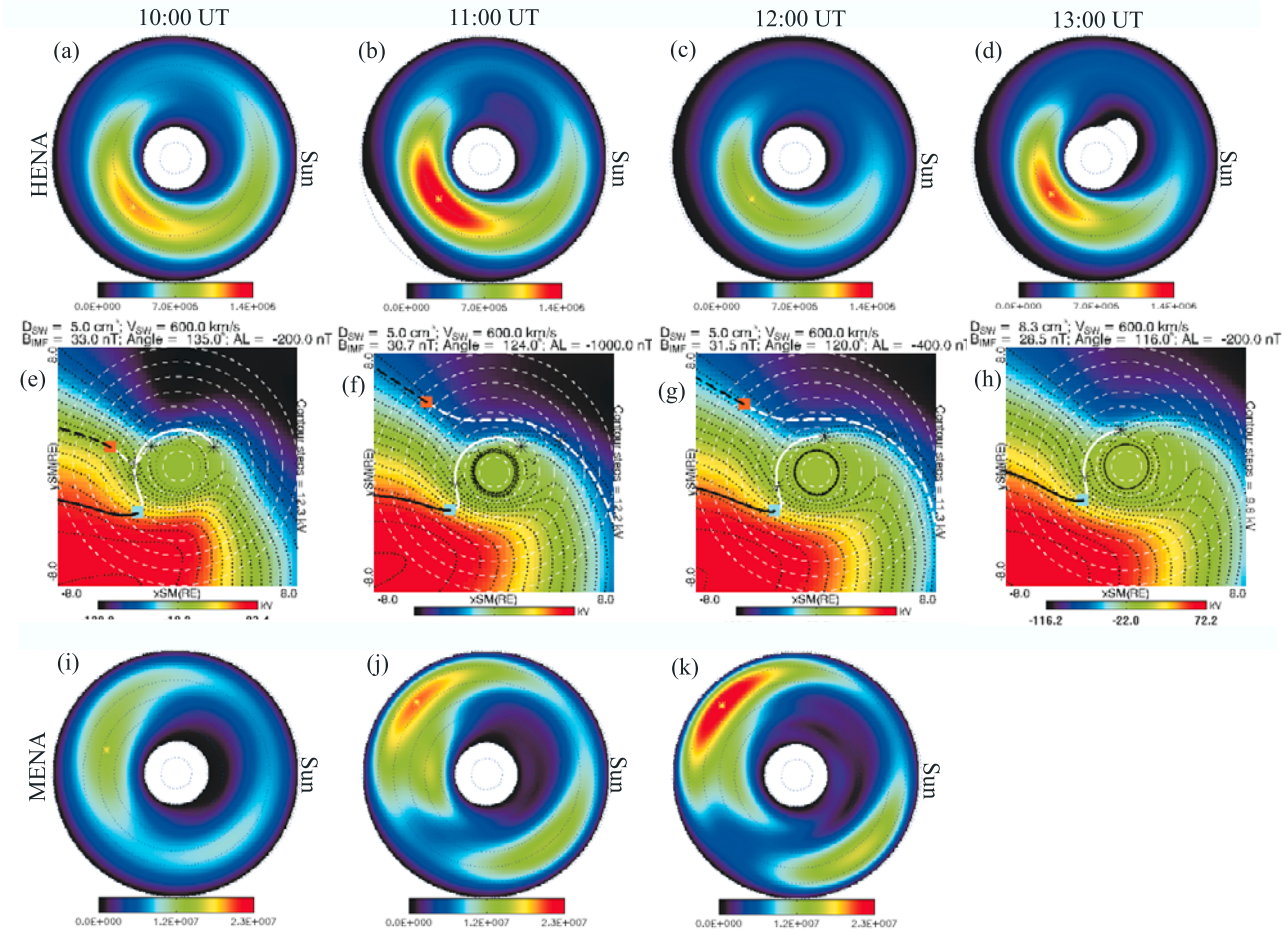

Figure 4. Same format as Figure 3 but for four hours on 12 August 2000.

corresponding speeds (blue and red solid lines). We also plot in the right-hand columns calculated speeds (dotted lines) that include the magnetic field gradient drift and the $\vec{E} \times \vec{B}$ drift speed. The electric field contains the corotational field and a convection field calculated from the Weimer 2001 [*Weimer*, 1996; *Weimer*, 2001] electric potential mapped from the ionosphere to the equator using the Tsyganenko 89 [*Tsyganenko*, 1989] magnetic field model. The curvature drift is omitted because we take the pitch angle to be 90° so that the ions stay at the equator.

[24] Error bars on the points in Figure 6 would be useful, but this is not possible. There are uncertainties in the data that are not known. There are uncertainties in the inversion process that are hard to quantify. Most important of all is that what is plotted is the position of a peak that is sometimes sharp and sometimes broad. Quantitative error bars are not possible.

[25] To understand this motion and to make quantitative comparisons with the predicted electric fields, Figures 3d–3f, Figures 4e–4h, and Figures 5d–5f are plotted. The color background shows the electric potential of the Weimer 2001 model for the solar wind and geomagnetic activity levels shown at the top of each panel. These values are rounded-off approximations to solar wind values. The black dotted lines are equipotential curves that are the sum of the Weimer potential and the corotational electric potential. The interval between the contours is listed on the right of the panels. The white dashed circles are at 1 R_E intervals to provide scale. The solid white lines show the predicted motion of a 33 keV ion guiding center with 90° pitch angle for 2 hours ahead assuming that the electric potential did not change. The solid black lines show the predicted motion of the same 33 keV ion for the 2 previous hours assuming that the electric potential did not change. The blue squares mark the initial location of the 33 keV peak at that time. One-hour intervals are marked by the black stars. The dashed white and black lines show the corresponding predicted motion for an 8.6 keV ion guiding center with 90° pitch angle. The brown/orange squares mark the initial location of the 8.6 keV peak. No loss mechanisms for the ions are included in the calculations.

[26] Since the observations presented here are not for a single energy but for a range of energies, 12 keV for HENA and 7 keV for MENA, and since the energy drift due to magnetic gradient and curvature is both energy and pitch angle distribution, the motion of a guiding center with the central energy in the band is only an approximate representation of the actual motion of the peak of the distribution. This is thought to be a valid simplification for the qualitative and semiquantitative results of this paper.

4.1. Drift During the Recovery Phase of the 10 June 2000 Storm

[27] Figure 6a shows that on 10 June 2000 for 2 hours during the recovery phase of this weak storm, i.e., between

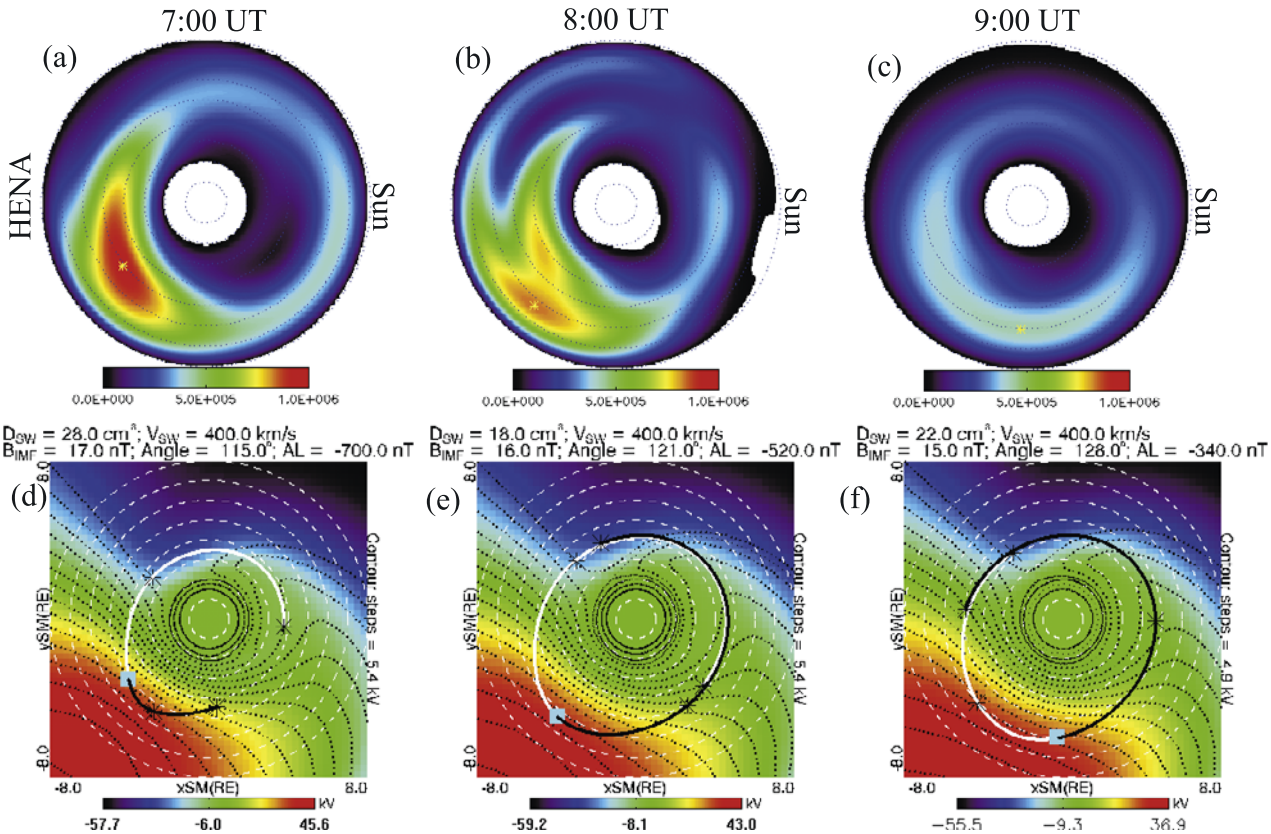

Figure 5. Same format as Figure 3 but for 4 October 2000 and with no 8.5 keV ion distributions.

1100 and 1300 UT, the peak in the 33 keV ions, which has already drifted from the night side to dusk, continues westward, but stops drifting and appears to turn back when it reaches noon. This, of course, is almost certainly not what happens. The ions seen between 1200 and 1300 UT are ions that were injected later and are now following similar drift paths to those observed between 1100 and 1200 UT. The fact that the ion flux decreases is probably a sign of ion loss either to decay mechanisms or through drift to the magnetopause.

[28] Figure 6b shows that between 1100 and 1200 UT the measured drift speed agrees with the model predictions. This is consistent with what was concluded by *Mitchell et al.* [2001] based on the ENA images and *Burch et al.* [2001a] from inversions of HENA images.

[29] Figure 3d shows that for ions injected in the tail to reach 4 R_E at dusk with 33 keV, they must have crossed a number of equipotential contours and thus have been injected at much lower energy. After reaching dusk they continue to drift without significant changes in kinetic energy, and thus are observed drifting under the influence of the magnetic gradient drift in this HENA energy channel. As can be see from Figures 3e and 3f, this model does not explain the decrease in strength of the ring current at this energy nor its apparent failure to continue to drift westward at the expected rate.

[30] Figure 6c shows that the peak flux of the 8.5 keV ions observed by MENA does not drift during this same period. Therefore as shown in Figure 6d, the inferred angular drift speed does not agree with the predictions of the model. Figures 3d–3f make it clear why. At 1100 and 1200 UT, ions of this energy that are injected in the tail region drift slowly westward crossing electric potential contours increasing their kinetic energy so that they are no longer seen by this MENA energy channel. At 1300 UT, the low energy ions drift slowly inward remaining in the postmidnight/predawn sector. The predicted angular speed moves much closer to the observed value. The stagnation of the injected ions at this time is also consistent with the increase in flux observed at 1300 UT.

[31] It is to be noted that during this time period which is in the early recovery phase of a weak storm, the 33 keV ions show an asymmetric ring current, and that the 8.5 keV ions are also weakly asymmetric. *Korth et al.* [2000] show that 100 keV ions as seen by CRRES reflect an asymmetric ring current and support *Grafe*'s [1999] conclusion that the ring current is almost always at least weakly asymmetric.

4.2. Drift Just After the Minimum in SYMH for the 12 August 2000 Storm

[32] Figure 6e shows that the peak in the 33 keV ions moves very little for 4 hours after the minimum in SYMH at 1000 UT in the strong storm on 12 August 2000. The predicted angular speed is larger and in the opposite direction from the observed angular speed as shown in Figure 6f. The model calculations in Figures 4e–4h make it clear why. Ions that reach 4 R_E in the postmidnight/predawn sector are being injected from the tail moving fairly closely along equipotential paths, but as they come closer to the Earth and their energy increases somewhat

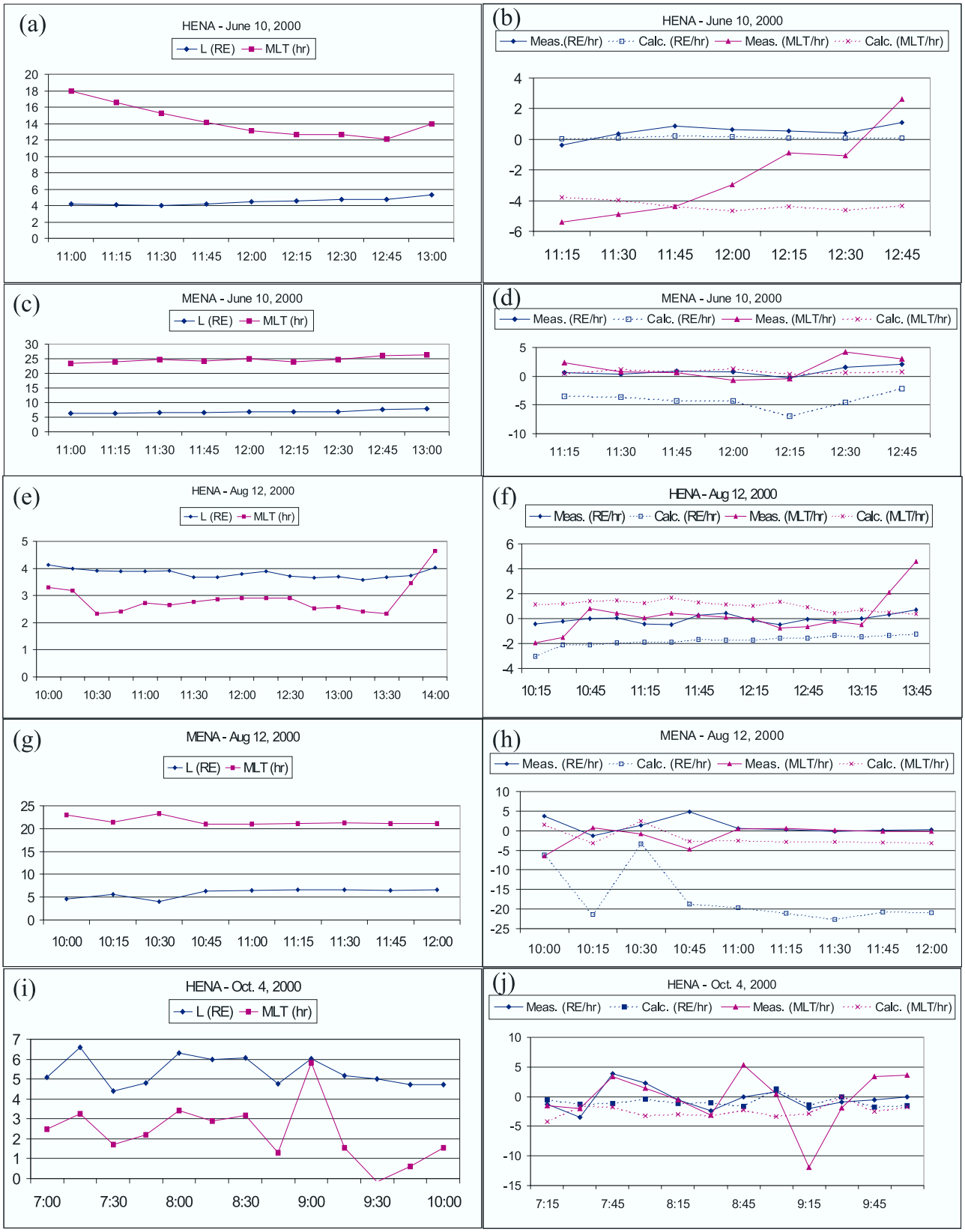

Figure 6. Plots of the radius (RE) and angular (MLT) positions of the peaks in the ion distributions as a function of time are shown in the left-hand column. Comparisons of the radial (RE/hour) and angular (MLT/hour) speeds of the peaks in the distributions and calculations using a Weimer 2001 electric field and a Tsyganenko 89 magnetic field.

and the magnetic gradient drift grows, the ions are pushed westward where they cross a number of equipotential lines, rapidly increasing their kinetic energy so that they are no longer seen in this HENA energy channel. Note that for the large polar cap potential for this storm, each equipotential line means a change in kinetic energy of approximately 10 keV. The rapid injection of the particles predicted in Figures 4e–4h is consistent with the findings of *Wygant et al.* [1998].

[33] In such a strong electric field, if 8.5 keV ions are to reach the inner magnetosphere, their guiding centers must closely follow equipotential lines because a change of 10 keV in kinetic energy would clearly take them out of this MENA energy band. The 8.5 keV ions at 1000 UT, i.e., Figure 4i, are predicted to move from just inside of 5 R_E to about 3 R_E as shown in Figure 4e but by this time they would have picked up enough kinetic energy to no longer be seen in this energy band. In Figure 4j, we see ions between 3 and 4 R_E near midnight as predicted. The peak 8.5 keV ion flux at 1100 and 1200 UT, see Figures 4j and 4k, is predicted to have been injected from the premidnight/postdusk sector from which it rapidly moves to the day side (see Figures 4f and 4g.) without crossing a number of equipotential surfaces. The local peak in 8.5 keV ion flux in the postdawn/prenoon sector may be the result of this drift.

[34] Using geosynchronous satellite data for 1996, *Korth et al.* [1999] found that for strong storms, $Kp > 6$, there were no 30 keV protons in the dusk region, whereas there were 10 keV ions. This is consistent with the ion distributions presented here. Studies of data from 1989–2000, however, do show that sometimes there were 30 keV ions on the dusk side (M. F. Thomsen, private communication, 2003). *Korth et al.* [1999] also find that 1 and 3 keV protons peaked more often at midnight and postmidnight which is consistent with MENA ENA images on 12 August 2000 at 1000 UT that were inverted in the work of *Perez et al.* [2001] and that show peaks near midnight.

[35] *C:son Brandt et al.* [2002c] showed postmidnight enhancements of the proton flux inferred from HENA observations in the 10–198 keV range. There were no clear westward dispersions of the peak with higher energy, which implies strong and skewed electric fields consistent with the self-consistent modeling performed by *Fok et al.* [2001].

[36] Using CRRES data, *Wygant et al.* [1998] observed electric fields that penetrate to 2.4 R_E during the main phase of strong storms but then were shielded from the inner magnetosphere to remain outside of 3.7 R_E by ring current ions during the recovery phase. We are observing the motion just after the end of the main phase at 1000 UT. The peak in the 27–39 keV ions moves in about 0.5 R_E from 1000 to 1300 UT then moves back out to 4.0 as shown in Figure 6e. Earthward movement of the inner edge of the 27–39 keV ions as shown in Figures 4a–4d is not discernable.

4.3. Drift Early in the Main Phase of Storm on 4 October 2000

[37] Figure 6i shows that the peak in the 33 keV ions obtained from the HENA images remains between 4 and 7 R_E and between 1 and 4 MLT for the time interval from 0700 to 0830 UT on 4 October 2000 after which it drifts toward midnight except for the anomalous location of the peak at 0900 UT (see next paragraph.). As shown in Figure 2, this is early in the main phase of the 4 October 2000 storm. As shown in Figure 6j, the predicted angular drift speed for this period is approximately 3 MLT/hour, much larger than is observed. The fact that the peak does not move but does seem to decay in strength is probably due to continuous injection during the early part of this period and then decay. Below we suggest that the "double" peak at 0800 UT may indicate a two-stage injection process.

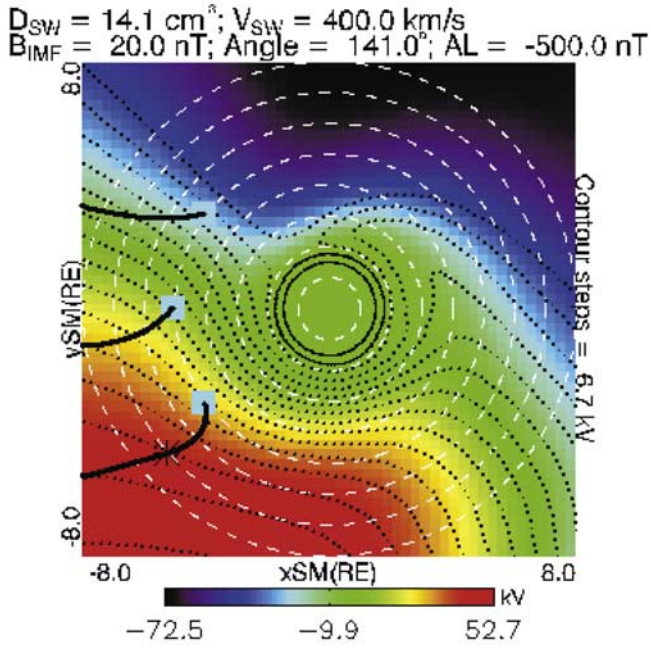

Figure 7. Plot of the drift motion of 33 keV ions backwards in time from three different initial locations on the nightside with solar wind and geomagnetic activity indices as input to the Weimer model appropriate for 0615 UT on 4 October 2000 rather than those for 0700 UT used in Figure 5d. The color contours and lines are explained in the text.

[38] Looking at Figures 5d–5f, it is clear that the ions are predicted to rapidly gain energy as they drift so as to no longer fall into this HENA energy band. However, if we use the predicted paths shown in Figures 5d–5f to determine whence these ions were injected, we find closed paths that do not originate in the plasma sheet. This begs the question as to their origin. Figure 7 plots the past history of 33 keV ions at the location of the observed peak at 0700 UT as well as at two other locations at the same radial distance. These paths do go back to the plasma sheet. The difference is that the parameters used in the Weimer 2001 electric field model are those appropriate for 0615 UT rather than 0700 UT. Comparing Figure 7 and Figure 5d and the solar wind and magnetic activity parameters listed there, we see that the differences are subtle and small. It is to be noted that *Wygant et al.* [1998] observed electric field variations on a 15 min to 1 hour time scale in the inner magnetosphere. Looking at GOES magnetic field data, *C:son Brandt et al.* [2002d] inferred induction electric fields of a few mV/m with variations on a similar time scale.

[39] As shown in Figure 5 the peak flux at 0900 UT is at dawn, whereas at times just before and after, Figure 6i shows that the peak is at 1–2 MLT. This sudden movement

of the peak is not what is expected. It is to be noted that there is a drop-off in proton intensity between 0800 and 0900 UT that is attributed to enhanced magnetospheric convection by *C:son Brandt et al.* [2002d]. The result is that the peak at 0900 UT is not very strong, and its position may reflect uncertainties in determining the location of peaks when the flux is low.

[40] Between 0900 and 1000 UT, inverting HENA 10–60 keV, ENA images with 6 min time resolution, *C:son Brandt et al.* [2002a] saw a substorm injection at 0922 UT which resulted in the ring current ions moving Earthward. The inversions of 27–39 keV ENA images done at 15 min intervals reported here show motion of the ion peak from 5.2 R_E to 4.7 R_E between 0915 and 1000 UT, consistent with the previous results.

[41] The fact that the peaks in the night side ring current are on the dawn side of midnight is consistent with calculations by *Fok et al.* [2001], observations of the electric fields in the inner magnetosphere by *Wygant et al.* [1998], and results by *C:son Brandt et al.* [2002c], who examined data from a number of storms and showed inverted HENA ENA images from the 4 October 2000 storm.

5. Summary and Conclusions

[42] We have observed the motion of ring current protons in the energy ranges 5–12 keV and 27–39 keV deduced from the MENA and HENA instruments on IMAGE during three storms in the year 2000. One was a 2 hour period during the recovery phase of a weak storm on 10 June 2000. A second was a 4 hour period just after the end of the main phase of a strong storm on 12 August 2000. The third was early in the long, main phase of a storm on 4 October 2000.

[43] Calculations of expected radial and angular drift speeds and the drift paths of the ions were made using a combination of the Tsyganenko 89 magnetic field model and the Weimer 2001 electric field model. In one case between 1000 and 1100 UT on 10 June 2000 that had already been reported, the westward drift of the 33 keV ions is as expected. Comparisons with speeds inferred from the motion of peaks in the ion distributions, however, often did not agree with the model predictions. Examination of the predicted paths showed that the ions are expected to experience significant energy changes as they drift so that they quickly move out of the observed energy channel. Unfortunately, the observed flux in higher energy ENA channels is not high enough to be able to perform effective inversions so that we are not able to observe the ions in these channels. The effects of particle losses are also not included in our analysis. Nevertheless, we are able to conclude that the observed motion is consistent with equatorial electric fields in the inner magnetosphere of a few tenths of a mV/m on 10 June 2000, several mV/m on 12 August 2000, and æ1 mV/m on 4 October 2000. These are the magnitudes predicted by the Weimer 2001 ionospheric electric potential model mapped to the equator using the Tsyganenko 89 magnetic field model. We do not have sufficient data for long enough times with enough energy resolution to confirm details of the spatial pattern of the electric fields. *Fok et al.* [2003] compare the motion of the ring current trapped ions using both the Weimer model and the CRCM model and find significant differences. For instance, simulations of the 4 October 2000 storm show better agreement with the HENA observations when the Rice Convection Model [*Harel et al.*, 1981] is used.

[44] Other interesting observations include (1) the suggestion of a two-step injection process during the main phase of the 4 October 2000 storm, (2) the unexplained disappearance of the 33 keV protons when their drift motion brings them to noon in the recovery phase of the 10 June 2000 storm, (3) the subtle changes in the electric potential pattern in the equator early in the 4 October 2000 storm that changes the predicted drift paths from ones in which particles are injected from the plasma sheet to closed orbits at 4–6 R_E, and (4) the energy dependence of the spatial source of the injected particles in the plasma sheet during the strong storm on 12 August 2000.

[45] **Acknowledgments.** We thank Robert Demajistre for assistance with the HENA instrument response function. This work has been partly funded by grants NAG512772 and ATM0302529.

[46] Lou-Chuang Lee thanks K. C. Hsieh and another reviewer for their assistance in evaluating this paper.

References

Barnett, C. F., et al. (1990), *Atomic Data for Fusion Collisions of H, H2, He, and Li Atoms and Ions With Atoms and Molecules*, Oak Ridge Natl. Lab., Oak Ridge, Tenn.

Burch, J. L. (2000), IMAGE mission overview, *Space Sci. Rev.*, *91*, 1.

Burch, J. L., et al. (2001a), View of Earth's magnetosphere with the IMAGE satellite, *Science*, *291*, 619.

Burch, J. L., D. G. Mitchell, B. R. Sandel, P. C:son Brandt, and M. Wüest (2001b), Global dynamics of the plasmasphere and ring current during magnetic storms, *Geophys. Res. Lett.*, *28*, 1159.

Chamberlain, J. W. (1963), Planetary coronae and atmospheric evaporation, *Planet. Space Sci.*, *11*, 901.

C:son Brandt, P., S. Barabash, O. Norberg, R. Lundin, E. C. Roelof, and C. J. Chase (1999), Energetic neutral atom imaging at low altitudes from the Swedish microsatellite Astrid: Images and spectral analysis, *J. Geophys. Res.*, *104*, 2367.

C:son Brandt, P., R. Demajistre, E. C. Roelof, S. Ohtani, D. G. Mitchell, and S. Mende (2002a), IMAGE/high-energy energetic neutral atoms: Global energetic neutral atom imaging of the plasma sheet and ring current during substorms, *J. Geophys. Res.*, *107*(A12), 1454, doi:10.1029/2002JA009307.

C:son Brandt, P., D. G. Mitchell, B. R. Sandel, J. L. Burch, and E. C. Roelof (2002b), Global IMAGE/HENA observations of the ring current: Examples of rapid response to IMF and plasmasphere interaction, *J. Geophys. Res.*, *107*(A11), 1359, doi:10.1029/2001JA000084.

C:son Brandt, P., S. Ohtani, D. G. Mitchell, M.-C. Fok, E. C. Roelof, and R. Demajistre (2002c), Global ENA observations of the storm main phase ring current: Implications for skewed electric fields in the inner magnetosphere, *Geophys. Res. Lett.*, *29*(20), 1954, doi:10.1029/2002GL015160.

C:son Brandt, P., S. Ohtani, D. G. Mitchell, R. Demajistre, and E. C. Roelof (2002d), ENA observations of a global substorm growth phase dropout in the nightside magnetosphere, *Geophys. Res. Lett.*, *29*(20), 1962, doi:10.1029/2002GL015057.

C:son Brandt, P., Y. Ebihara, S. Barabash, and E. C. Roelof (2002e), Energetic neutral atom images of a narrow flow channel from the plasma sheet: Astrid-1 observations, *J. Geophys. Res.*, *107*(A10), 1273, doi:10.1029/2001JA000230.

C:son Brandt, P., E. C. Roelof, S. Ohtani, D. G. Mitchell, and B. Anderson (2004a), IMAGE/HENA: Pressure and current distributions during the 1 October 2002 storm, *Adv. Space Res.*, in press.

C:son Brandt, P., D. G. Mitchell, R. Demajistre, E. C. Roelof, S. Ohtani, J. M. Jahn, C. J. Pollock, and G. Reeves (2004b), Storm-substorm relationships during the 4 October 2000 storm: IMAGE global ENA imaging results, in *Disturbances in Geospace: The Storm-Substorm Relationship*, *Geophys. Monogr. Ser.*, vol. 142, edited by A. S. Sharma, Y. Kamide, and G. S. Lakhina, AGU, Washington, D. C.

deBoor, C. (1978), *A Practical Guide to Splines*, Springer-Verlag, New York.

Fok, M. C., R. A. Wolf, R. W. Spiro, and T. E. Moore (2001), Comprehensive computational model of Earth's ring current, *J. Geophys. Res.*, *106*, 8417–8424.

Fok, M.-C., et al. (2003), Global ENA IMAGE simulations, *Space Sci. Rev.*, *109*, 77–103.

Grafe, A. (1999), Are our ideas about Dst correct?, *Ann. Geophys.*, *17*, 1.

Gruntman, M. (1997), Energetic neutral atom imaging of space plasmas, *Rev. Sci. Instrum.*, *68*, 3617.

Harel, M., R. A. Wolf, P. H. Reiff, R. W. Spiro, W. J. Burke, F. J. Rich, and M. Smioddy (1997), Quantitative simulation of a magnetospheric substorm: 1. Model logic and overview, *J. Geophys. Res.*, *86*, 2217–2241.

Hedin, A. E. (1991), Extension of the MSIS thermospheric model into the middle and lower atmosphere, *J. Geophys. Res.*, *96*, 1159.

Henderson, M. G., G. D. Reeves, H. E. Spence, R. B. Sheldon, A. M. Jorgensen, J. B. Blake, and J. F. Fennell (1997), First energetic neutral atom images from Polar, *Geophys. Res. Lett.*, *24*, 1167.

Henderson, M. G., G. D. Reeves, K. R. Moore, H. E. Spence, A. M. Jorgensen, J. F. Fennell, J. B. Blake, and E. C. Roelof (1999), Energetic neutral atom imaging with the POLAR CEPPAD/IPS instrument: Initial forward modeling results, *Phys. Chem. Earth C*, *24*, 203–208.

Iyemori, T. (1990), Storm-time magnetospheric currents inferred from mid-latitude geomagnetic field variations, *J. Geomagn. Geoelectr.*, *42*, 1249.

Jorgensen, A. M., H. E. Spence, M. G. Henderson, G. D. Reeves, M. Sugiura, and T. Kamei (1997), Global Energetic Neutral Atom (ENA) measurements and their association with the Dst index, *Geophys. Res. Lett.*, *24*, 3173.

Jorgensen, A. M., L. Kepko, M. G. Henderson, H. E. Spence, G. D. Reeves, J. B. Sigwarth, and L. A. Frank (2000), Association of energetic neutral atom bursts and magnetospheric substorms, *J. Geophys. Res.*, *105*, 18,753.

Korth, A., R. H. W. Friedel, C. G. Mouikis, J. F. Fennell, J. R. Wygant, and H. Korth (2000), Comprehensive particle and field observations of magnetic storms at different local times from the CRRES spacecraft, *J. Geophys. Res.*, *105*, 18,729.

Korth, H., and M. F. Thomsen (2001), Plasma sheet access to geosynchronous orbit: Generalization to numerical global field models, *J. Geophys. Res.*, *106*, 29,655.

Korth, H., M. F. Thomsen, J. E. Borovsky, and D. J. McComas (1999), Plasma sheet access to geosynchronous orbit, *J. Geophys. Res.*, *104*, 25,047.

Mitchell, D. G., et al. (2000), High Energy Neutral Atom (HENA) imager for the IMAGE mission, *Space Sci. Rev.*, *91*, 67.

Mitchell, D. G., K. C. Hsieh, C. C. Curtis, D. C. Hamilton, H. D. Voss, E. C. Roelof, and P. C:son Brandt (2001), Imaging two geomagnetic storms in energetic neutral atoms, *Geophys. Res. Lett.*, *28*, 1151.

Ostgaard, N., S. B. Mende, H. U. Frey, G. R. Gladstone, and H. Lauche (2003), Neutral hydrogen density profiles derived from geocoronal imaging, *J. Geophys. Res.*, *108*(A7), 1300, doi:10.1029/2002JA009749.

Perez, J. D., M.-C. Fok, and T. E. Moore (2000), Deconvolution of energetic neutral atom images of the Earth's magnetosphere, *Space Sci. Rev.*, *91*, 421.

Perez, J. D., G. Kozlowski, P. C:son Brandt, D. G. Mitchell, J.-M. Jahn, C. J. Pollock, and X. X. Zhang (2001), Initial ion equatorial pitch angle distributions from medium and high energy neutral atom images obtained by IMAGE, *Geophys. Res. Lett.*, *28*, 1155.

Pollock, C. J., et al. (2000), Medium Energy Neutral Atom (MENA) imager for the IMAGE mission, *Space Sci. Rev.*, *91*, 113.

Pollock, C. J., et al. (2001), First medium energy neutral atom (MENA) images of Earth's magnetosphere during substorm and storm time, *Geophys. Res. Lett.*, *28*, 1147.

Press, W. H., B. P. Flannery, S. A. Teukolsky, and W. T. Vettering (1992), *Numerical Recipes*, 2nd ed., Cambridge Univ. Press, New York.

Roelof, E. C. (1987), Energetic neutral atom image of a storm-time ring current, *Geophys. Res. Lett.*, *14*, 652.

Roelof, E. C., and A. J. Skinner (2000), Extraction of ion distributions from magnetospheric ENA and EUV images, *Space Sci. Rev.*, *91*, 437.

Stancil, P. C., D. R. Schultz, M. Kimura, J.-P. Gu, G. Hirsch, and R. J. Buenker (1999), Charge transfer in collisions of O^+ with H and H^+ with O, *Astron. Astrophys. Suppl. Ser.*, *240*, 225.

Tsyganenko, N. A. (1989), A mangnetospheric magnetic field model with a warped tail current sheet, *Planet. Space Sci.*, *37*, 5.

Tsyganenko, N. A. (1995), Modeling the Earth's magnetospheric magnetic field confined within a realistic magnetopause, *J. Geophys. Res.*, *100*, 5599–5612.

Wahba, G. (1990), *Spline Models for Observational Data*, Soc. for Ind. and Appl. Math., Philadelphia, Penn.

Weimer, D. R. (1996), A flexible IMF dependent model of high-latitude electric potentials having "space weather" applications, *Geophys. Res. Lett.*, *23*, 2549.

Weimer, D. R. (2001), An improved model of ionospheric electric potentials including substorm perturbations and application to the Geospace Environment Modeling November 24, 1996, event, *J. Geophys. Res.*, *106*, 407.

Whipple, E. C., et al. (1998), Identification of magnetospheric particles that travel between spacecraft and their use to help obtain magnetospheric potential distributions, *J. Geophys. Res.*, *103*, 93.

Whipple, E. C., D. L. Starr, J. S. Halekas, J. D. Scudder, R. D. Holdaway, J. B. Faden, P. Puhl-Quinn, N. C. Maynard, and C. T. Russell (1999), Magnetospheric electric fields from ion data, *Geophys. Res. Lett.*, *26*, 1561.

Williams, D. J., E. C. Roelof, and D. G. Mitchell (1992), Global magnetospheric imaging, *Rev. Geophys.*, *30*, 183.

Wygant, J., D. Rowland, H. J. Singer, M. Temerin, F. Mozer, and M. K. Hudson (1998), Experimental evidence on the role of the large spatial scale electric field in creating the ring current, *J. Geophys. Res.*, *103*, 29,527.

P. C:son Brandt and D. G. Mitchell, Applied Physics Laboratory, Johns Hopkins University, Laurel, MD 20723, USA. (brandpc1@jhuapl.edu; donald.g.mitchell@jhuapl.edu)

J.-M. Jahn and C. J. Pollock, Space Science Department, Southwest Research Institute, 6220 Culebra Road, San Antonio, TX 78238-5166, USA. (jjahn@swri.edu; cpollock@swri.edu)

J. D. Perez, Physics Department, Auburn University, Auburn, AL 36849, USA. (perez@physics.auburn.edu)

X.-X. Zhang, Center for Space Plasma and Aeronomy Research, University of Alabama in Huntsville, Huntsville, AL 35899, USA. (zhangx@cspar.uah.edu)